Herraiz Cardona, I.; Ortega Navarro, EM.; Garcia-Anton, J.; Pérez-Herranz, V. (2011). Assessment of the roughness factor effect and the intrinsic catalytic activity for hydrogen evolution reaction on Ni-based electrodeposits. International Journal of Hydrogen Energy. 36(16):9428-9438. doi:10.1016/j.ijhydene.2011.05.047.

Assessment of the Roughness Factor Effect and the Intrinsic Catalytic Activity for Hydrogen Evolution Reaction on Ni-based Electrodeposits

I. Herraiz-Cardona, E. Ortega, J. García Antón, V. Pérez-Herranz*

IEC Group. Departamento de Ingeniería Química y Nuclear. Universidad Politécnica de Valencia. Camino de Vera s/n. 46022 Valencia, Spain.

*Corresponding author. Tel.: +34-96-3877632; fax: +34-96-3877639;

e-mail address: vperez@iqn.upv.es (V. Pérez-Herranz)

Abstract

The hydrogen evolution reaction (HER) was studied in 30 wt.% KOH solution at temperatures ranging between 30 and 80 ºC on three type of electrodes: (i) rough pure Ni electrodeposits, obtained by applying a large current density; (ii) smooth NiCo electrodeposits; (iii) smooth commercial Ni electrodes. By using steady-state polarization curves and electrochemical impedance spectroscopy (EIS) the surface roughness factor and the intrinsic activities of the catalytic layers were determined. These techniques also permitted us to determine the mechanism and kinetics of the HER on the investigated catalysts. Different AC models were tested and the appropriate one was selected. The overall experimental data indicated that the rough/porous Ni electrode yields the highest electrocatalytic activity in the HER. Nevertheless, when the effect of the surface roughness was taken into consideration, it was demonstrated that alloying Ni with Co results in an increased electrocatalytic activity in the HER when comparing to pure Ni. This is due to an improved intrinsic activity of the material, which was explained on the basis of the synergism among the catalytic properties of Ni (low hydrogen overpotential) and of Co (high hydrogen adsorption).

Keywords: Porous Ni Electrodeposits, NiCo Alloys, Surface Roughness Factor, Electrochemical Impedance Spectroscopy.

1. Introduction

Hydrogen is considered an ideal energy carrier that can be an alternative to fossil fuels. It is a clean and fully recyclable substance with a practically unlimited supply, and has all the criteria considered for an alternative energy source. The electrochemical production of hydrogen by alkaline water electrolysis is one of the most promising methods with great potential of using renewable energy sources. Moreover, it represents an environmentally friendly technology for production of high purity hydrogen [1-5]. However, the high energy consumption of alkaline water electrolysers restrains its large-scale application at present. Although platinum shows the highest activity for the hydrogen evolution reaction (HER), new electrode materials have been investigated, aiming at the reduction of the cost associated with the electrocatalyst development. Among these materials, nickel and its alloys show a high initial electrocatalytic activity toward the HER [6-8]. The electrode activity can be enlarged by increasing the real surface area and/or the intrinsic activity of the electrode material [9].

The increase of the real surface area can be achieved by several methods: depositing Ni together with an active metal like Al or Zn (i.e. by pressing [10, 11], electrodeposition [12-17], composite coating [18-20], and thermal spray [6]) followed by the dissolution of the secondary component (Raney type electrodes); electrodeposition of Ni at large current densities [21-23]; electrodeposition of Ni on metallic opals (made of silica or polystyrene) with proper porosities and layer/thickness, followed by a selective removal of the opal [24]. As a result, a porous, three-dimensional structure is obtained, characterized by a high surface roughness factor, R_f. On the other hand, the intrinsic activity of Ni has been enlarged by alloying Ni with some metals: NiCo [12, 17, 25, 26]; NiLa [27, 28]; NiMo [8, 29, 30]; NiW [29, 31]; NiFe [29, 32].

In this work, two different Ni-based coatings electrodeposited on AISI 304 stainless steel have been developed: a pure Ni catalyst provided with a large surface roughness obtained by applying a high current density (Ni-Hcd catalyst); and a smooth nickel-cobalt alloy (NiCo catalyst). The aim of the present work is to study the electrocatalytic performance of the developed electrodes for HER, distinguishing the effect of both the surface roughness and the intrinsic activity of the material, by the determination of the real active surface area of the catalyst, in terms of R_f. The mechanisms and kinetics of the HER on these electrodes have also been determined. Experimental data were obtained in 30 wt. % KOH solution by using steady state polarization curves and electrochemical impedance spectroscopy (EIS) techniques.

2. Experimental

2.1 Preparation of electrodes

The metallic coatings were deposited on an AISI 304 stainless steel substrate, embedded in Teflon, leaving a cross-sectional available area of 0.5 cm^2. AISI 304 stainless steel as substrate material was mainly chosen due to its good mechanical and corrosion resistance at relatively low cost.

Before the electrodeposition experiments the stainless steel substrate was mechanically polished with emery paper down to 4000 grit, next it was degreased for 1 minute with 25 wt.% NaOH at 90 ºC, immersed in HCl 18 wt.% during 1 minute and anodically treated in 70 wt.% H_2SO_4 at 1080 A m^{-2} for 3 minutes. Then, the substrate surface was struck at 268 A m^{-2} in a Wood's nickel solution (240 g L^{-1} $NiCl_2$, 120 mL L^{-1} HCl) for 5 minutes, in order to produce a thin, adherent deposit of nickel which serves as a base for the subsequent electrodeposition. Between each treatment the electrode was rinsed with distilled water. The formation of electroactive coatings on such prepared AISI 304 stainless steel substrate was done by electrodeposition at a constant current from the corresponding salt baths. The bath composition and deposition conditions are listed in Table 1. After the deposition of the active electrocatalyst material, the electrode surface was carefully rinsed with a large amount of distilled water in order to remove any residues of bath chemicals.

Electrodepositions were carried out in a thermostated one-compartment cell made of Pyrex glass with a Teflon cover having adequate holes to lodge the electrodes and entrances to add reagents to the bath. The solution inside the cell had an initial volume of 50 mL and was agitated by means of a magnetically driven stirrer. The counter electrode was a large-area platinum electrode. The reference electrode was a commercially available silver-silver chloride (Ag-AgCl) electrode with 3 M potassium

chloride (KCl) solution. The experiments were accomplished by using an AUTOLAB PGSTAT302N potentiostat/galvanostat.

The structures, morphologies and compositions of the Ni-Hcd and NiCo alloys were examined by means of a JEOL JSM-3600 scanning electron microscope.

2.2 Electrochemical measurements

The developed electrodes were characterized by means of steady-state polarization curves and EIS. All these tests were performed in oxygen free 30 wt.% KOH solutions which were achieved by bubbling N_2 for 15 min before the experiments.

Polarization curves were potentiodynamically recorded from -1.60 V vs Ag/AgCl (-1.40 V vs SHE) up to the equilibrium potential at a scan rate of 1 mV s^{-1}, and at six different temperatures: 30, 40, 50, 60, 70 and 80ºC. Before the tests, the working electrode was held at -1.60 V (vs $V_{Ag/AgCl}$) in the same solution in order to reduce the oxide film existing on the surface electrode layer, for the time needed to establish reproducible polarization diagrams.

EIS measurements were performed after obtaining the polarization curves. Alternating current impedance measurements were carried out at different cathodic overpotentials, and at the following temperatures: 30, 50, and 80 ºC. The measurements were made in the frequency range of 10 kHz to 3 mHz. Ten frequencies per decade were scanned using a sinusoidal signal of 10 mV peak-to-peak. The complex nonlinear least square (CNLS) fitting of the impedance data was carried out with the Zview 3.0 software package.

The electrochemical measurements were carried out in an electrochemical cell developed by the Dpto. Ingeniería Química y Nuclear of the Polytechnic University of Valencia [33]. It is a three-electrode cell with a heating circuit to control the

temperature. A Luggin capillary, whose tip was set at a distance of about 1 mm from the surface of the working electrodes, was used to minimize the variations due to *jR* drop in the electrolyte. In this system, the developed electrodes were used as the working electrodes, a large-area platinum electrode was employed as counter electrode, and the reference electrode was the same as that used in the electrodepositon process. The electrochemical experiments were performed using an AUTOLAB PGSTAT302N potentiostat/galvanostat.

3. Results and discussion

3.1 Morphology of Ni-Hcd and NiCo electrodes

The SEM micrographs, shown in Fig.1, illustrate the extend morphology of the electrodeposits obtained according to the experimental conditions reported in Table 1. As it is clear from Fig. 1, the superficial morphology of the two developed catalyst is very different. On the one hand, the Ni-Hcd catalyst consists of a continuous matrix with cavities and pores distributed in the whole surface (Fig. 1.a). On the other hand, the NiCo alloy shows a smooth superficial layer (Fig. 1.b).

The macroporosity of the Ni-Hcd layer is originated by the random nucleation of the dissolved hydrogen, which produces microbubbles attached to the electrode surface, as a consequence of the high current densities applied. The electrodeposition process takes place in the free area and cavities are produced, where hydrogen generated in the neighbourhood continues draining [21]. Quasy-cylindrical pores, whose diameter is mainly determined by the gas-liquid interfacial tension (157 ± 23 μm), are obtained in this way. In contrast, with respect to the NiCo alloy, the low current density applied in the electrodeposition experience results in a homogeneous smooth surface.

The studied electrodes also differ in the superficial composition: whereas the Ni-Hcd catalyst is conformed by a pure Ni layer, the NiCo alloy has a Co content of 47.7 wt.%.

3.2 Polarization measurements

In order to investigate the catalytic activity of the prepared layers, Tafel linear polarization measurements were performed in 30 wt.% KOH solution, and the corresponding electrochemical parameters (Tafel slope, exchange current density, transfer coefficient) were derived from the recorded curves. Fig. 2 shows a set of Tafel

curves recorded at 50 ºC on the two catalyst layers investigated. A curve performed on commercial smooth Ni electrode was also included to compare the obtained results. The curves were corrected with respect to the reversible HER potential at the given conditions and for the *jR*-drop. The Tafel curves obtained for both NiCo and Ni-Hcd layers (Fig. 2) show a classical Tafelian behaviour, indicating that the HER on these electrodes is a purely kinetically controlled reaction described by the Tafel equation [29, 34]:

$$\eta = a + b \log j \tag{1}$$

where η (V) represents the applied overpotential, j (A cm^{-2}) the resulting (measured) current density, b (V decade^{-1}) the Tafel slope, and a (V) is the intercept related to the exchange current density j_0 (A cm^{-2}) through equation:

$$a = (2.3RT)/(\beta n_e F) \times \log j_0. \tag{2}$$

The other parameter of interest is β, the symmetry factor, which can be calculated from the Tafel slope as

$$b = -(2.3RT)/(\beta n_e F), \tag{3}$$

and n_e represents the number of electrons exchanged, F (=96,485 C mol^{-1}) is the Faraday constant, and R (= 8.314 J mol^{-1} K^{-1}) is the gas constant. Since both Ni-Hcd and NiCo curves in Fig. 2 do not show any significant change in the Tafel slope, the same HER reaction mechanism should be valid through the entire overpotential region investigated. The values of the kinetic parameters are reported in Table 2. The mechanism of HER in alkaline solution involves the formation of an adsorbed hydrogen atom (adatom) intermediate, MH_{ads} (Volmer reaction, Eq. (4)), the electrodic desorption of hydrogen into solution (Heyrovsky reaction, Eq. (5)) and/or a chemical desorption by the combination of two adatoms (Tafel reaction, Eq. (6)):

$$H_2O + M + e^- \rightarrow MH_{ads} + OH^- \quad (4)$$

$$H_2O + MH_{ads} + e^- \rightarrow H_2 + M + OH^- \quad (5)$$

$$MH_{ads} + MH_{ads} \rightarrow H_2 + 2M \quad (6)$$

where M is a free site on the metal surface and MH_{ads} is the metal surface occupied by hydrogen adatoms. When the mechanism is determined from the rate-determining step (rds) of a multi-step reaction, the Tafel slope plays an important role in estimating the mechanism [35, 36]. It has been widely accepted that the value of the charge-transfer coefficient, α, depends on the rds for multi-step reactions [10, 11, 13, 37, 38]. Note that for the Volmer step the symmetry factor, β, is equal to the transfer coefficient, α (i.e. $\alpha = \beta$), while for the Heyrovsky step the transfer coefficient is equal to $\alpha = 1+\beta$ [34, 39]. According to the general model for the HER mechanism, when the rds is Eq. (4), or Eq (4) coupled with Eq (5), or Eq (4) coupled with Eq (6), the value of α is 0.5. Therefore, the Tafel slope becomes 120 mV dec^{-1} at 30 ºC, and 140 mV dec^{-1} at 80 ºC. Other possibilities are $\alpha = 1.5$ and $b = 40$ mV dec^{-1} at 30 ºC, when Eq. (5) is rds; and $\alpha = 2$ and $b = 30$ mV dec^{-1} at 30 ºC, when Eq. (6) is the rds [40-42]. Here, the Tafel slope ranges between 100 mV dec^{-1} and 150 mV dec^{-1} at 30 and 80 ºC, respectively, and the $\alpha = \beta$ values are very close to 0.5 for the two developed electrodes (see Table 2). Therefore, following the criteria mentioned above, one can assume that the Volmer step must control the HER on Ni-Hcd and NiCo electrodes.

In contrast to the behaviour reported for the developed electrodes, the polarization curves recorded on the smooth Ni electrode (Fig. 2) display two potential-dependent regions related to the HER. The slope decreases from higher values at overpotentials less cathodic than approximately - 200 mV to lower values at more

cathodic overpotentials. The existence of two Tafel regions has already been reported in literature on Ni-based catalysts [22, 28, 37, 41, 43-45]. At low cathodic overpotentials the Tafel slopes are higher than 120 mV dec^{-1} at 30 ºC, which may indicate the presence of some oxides on the surface of the Ni electrode [29, 44].

In Table 2 it is also reported the overpotential values at a fixed current density of -100 mA cm^{-2}, η_{100}. This parameter gives an indication on the amount of energy (overpotential) that has to be invested to produce a fixed amount of hydrogen. The current efficiency of the process, determined from the hydrogen volume measured with the aid of the electrochemical cell [33], is about 99.9 %. The developed electrodes are characterized by higher exchange current density, j_0, and lower hydrogen overpotential, η_{100}, compared to the smooth Ni electrode, thereby indicating an improvement of electrocatalytic activity. In addition, a significant increase of catalytic efficiency is evidenced for the Ni-Hcd electrode, that exhibits the lowest values of η_{100}, and the highest values of j_0.

The information obtained from the Tafel polarization data demonstrate that the investigated Ni-based catalysts are very active for the HER, showing a higher catalytic activity than the smooth Ni electrode. Ni-Hcd has shown to be the best overall catalyst. However, since the Tafel curves are normalized to the geometric area of the catalysts and not to the real electrochemical area, the results discussed above cannot offer a definite conclusion if the observed electrocatalytic activity is a result of only an increased surface area of the catalysts, or if an improvement in the intrinsic (electronic) electrocatalytic properties of the catalyst material is also a contributing factor. Therefore, in order to obtain information on the intrinsic activity of the investigated layers in the HER, the curves presented in Fig. 2 should be normalized to the real electrochemically active surface area. In this work, an EIS technique has been proposed

as the most appropriate to determine the real surface area in electrochemical systems, as previously used in literature [6, 46]. Thus, the following section of the paper will discuss the EIS results obtained on the catalytic layers developed.

3.3 Electrochemical Impedance Spectroscopy Measurements

To ensure a complete characterization of the electrode/electrolyte interface and corresponding processes, EIS measurements were made at different selected overpotentials of the previously obtained polarization curves: η_1, corresponding to the equilibrium potential, 0 mV; η_2, a cathodic overpotential at which it is not manifested the hydrogen evolution; η_3, an overpotential at which the hydrogen production takes place at a very low rate; and η_4, at which hydrogen is vigorously generated. Figures 3 and 4 show examples of EIS spectra recorded on the Ni-Hcd and NiCo electrocatalysts, respectively. The EIS spectra recorded on the Ni-Hcd catalyst (Fig.3) reveal the presence of two overlapped semicircles (i.e. two different time constants), the first one at high frequencies (HF), and the second one, at low frequencies (LF). From Fig.3 it is clear that the diameter of the LF semicircles diminishes considerably with both the cathodic overpotential and the temperature, whereas the diameter of the HF semicircle remains almost unchanged. With respect to the impedance spectra of the NiCo electrode, it is shown in Fig. 4 that the two semicircles are strongly overlapped, appearing only one maximum in the Bode representation (Fig. 4.a.2 and 4.b.2). The Nyquist plots of the impedance of the NiCo layer show that the diameter of the LF semicircle presents the same behaviour as that reported for the Ni-Hcd electrode. On the other hand, for the NiCo electrocatalyst the diameter of the HF semicircle remains almost constant with the overpotential, diminishing considerably with temperature, as it is clear from Fig. 4.b.1. In addition to this, we observe for both the Ni-Hcd and the

NiCo electrocatalysts, that at high overpotentials (η_4) the LF capacitive loop disappears and it is shown an inductive loop at LF in the Nyquist plots (see the inset in Fig. 3.a.1 and Fig. 4.a.1). The LF inductive loop for hydrogen evolution reaction has been early proposed by Conway and co-workers [47] and later experimentally observed by other authors for Ni-Zn [38] and Ni-P [48] in alkaline media. These workers also found significant absorption of hydrogen and formation of surface hydride layers in these systems. The reason for the observed inductive behaviour may be due to the hydride formation at these overpotentials [47-49].

In order to derive a physical picture of the electrode/electrolyte interface and the processes occurring at the electrode surface, two different electric equivalent circuit (EEC) models have been used to fit the EIS response of the catalysts investigated (Fig. 5): (a) the two-time constant parallel model (2TP); and (b) the two-time constant serial model (2TS).

The 2TP model (Fig. 5a) represents a slightly modified model originally proposed by Armstrong and Henderson [50], in which the double layer capacitance was replaced by a constant phase angle element (CPE) [43, 51]. CPE is defined in impedance representation as:

$$Z_{CPE} = \left[Q \cdot (i \cdot \omega)^n\right]^{-1} \tag{7}$$

where Q is the CPE constant, ω is the angular frequency (in rad/s), $i^2 = -1$ is the imaginary unity and n is the CPE exponent. The CPE element is a widely-used empirical element to account for the non-ideal behaviour of the capacitive elements due to different physical phenomena such as surface heterogeneity which results from surface roughness, impurities, dislocations or grain boundaries [52]. The 2TP model reflects the response of a HER system characterized by two semicircles (i.e. two time constants): the HF semicircle, τ_1 (CPE_1-R_1), related to the charge transfer kinetics, and

the LF semicircle, τ_2 $(CPE_2\text{-}R_2)$, related to the hydrogen adsorption [12, 29, 51, 53, 54]. It is important to note that, in this case, the diameter of both the HF and the LF semicircles change with overpotential (i.e. the two time constants change with overpotential). The 2TS model (Fig. 5b), proposed by Chen and Lasia [10], similarly to the 2TP model, reflects the response of a HER system characterized by two semicircles, but only the LF semicircle is related to the kinetics of the HER. The time constant associated to this semicircle, τ_2 $(CPE_2\text{-}R_2)$, changes with overpotential. The HF semicircle is associated to the porosity of the electrode surface [7, 51, 55, 56], and the time constant related to this semicircle, τ_1 $(CPE_1\text{-}R_1)$, does not change with overpotential. According to the discussion presented above, the suitability of a specific EEC to model the experimental data can be considered as a criterion to prescribe parameters to the specific processes (i.e. charge transfer kinetics, surface porosity or hydrogen adsorption).

To model the experimental data of the impedance response characterized by two semicircles in the Nyquist plot (i.e. recorded at the overpotentials η_1, η_2, and η_3) both two-time constant EEC models were tested. Fig. 3 shows that a very good agreement between the experimental (symbols) and CNLS approximations (lines) data is obtained when the 2TS model is used to describe the EIS response of the Ni-Hcd layer at the overpotentials η_1, η_2, and η_3. The 2TP model was also successfully used to model EIS spectra on this electrode. By formal statistical analysis, it is impossible to distinguish between the 2TP and 2TS models in this case, what was confirmed by the sequential *F*-test. Hence, it is necessary to examine the obtained values of the circuit elements of the two EEC models, and conclude on the trend in overpotential behavior.

Table 3 shows the best-fit estimates of the different EEC parameters obtained from the impedance measurements of both the Ni-Hcd and NiCo electrode at different

temperatures. The average double layer capacitances, C_i, for the catalytic coatings were determined using the relation suggested by Brug et al. [57]:

$$C_i = [Q_i / (R_S^{-1} + R_i^{-1})^{(1-n_i)}]^{1/n_i} \quad (8)$$

From Table 3 it is clear that for the Ni-Hcd electrocatalyst, when the 2TS EEC model is used to model the experimental data, the first time constant, τ_1 *(CPE$_1$-R$_1$)* or HF time constant, diminishes very slightly with both overpotential and temperature, maintaining this parameter in the same order of magnitude. In fact, in the impedance data plotted in Fig. 3, the diameter of the HF semicircle is practically constant for the overpotential values that present a two-time constant response. The value of Q_1 decreases with the overpotential, increasing at the same time the value of R_1. This behaviour is associated with the response of the pores [58]. Hence, on the basis of the overpotential behaviour of these two parameters, it could be concluded that the first time constant, τ_1 *(CPE$_1$-R$_1$)* or HF time constant, is related to the surface porosity. By contrast, τ_2 varies until two orders of magnitude with overpotential, and both the Q_2 and the R_2 decrease with overpotential. So, it could be concluded that the second time constant, τ_2 *(CPE$_2$-R$_2$)* or LF time constant, is related to the HER charge-transfer kinetics, namely to the response of double layer capacitance characterized by *CPE$_2$*, and HER charge transfer resistance characterized by R_2. From these observations one can conclude that the 2TS EEC properly models and describes the AC response of the Ni-Hcd layers.

With respect to the NiCo catalytic coating, due to the fact that the two semicircles are strongly overlapped, it was very difficult to determine which initialization values of the EEC parameters ensure a correct convergence. For this reason it was necessary to recur to other graphical methods to save the limitations of the

usual methods used for representing the impedance data. Orazem et al. [59] proposed a graphical approach to estimate the values of the CPE coefficients (*n* and *Q*). The CPE exponent, *n*, can be obtained from the high-frequency slope of the imaginary part of the impedance on a logarithmic scale, as it is shown in Fig. 6. Moreover, an effective CPE coefficient, Q_j, may be obtained directly from the imaginary part of the impedance as

$$Q_j = \sin\left(\frac{n_i\pi}{2}\right)\frac{-1}{Z''(f)(2\pi f)^{n_i}}. \quad (9)$$

Fig.7 shows the effective CPE coefficients determined by using Eq. 9. The asymptotic values obtained at high-frequencies provide correct values for the CPE coefficient, Q_1, and they have been reported on Table 3. Once fixed these two parameters, the approximation fitting to the impedance data with both two-time constant EEC was successfully carried out by using the ZView software. As it is clear from Fig. 8, the use of the 2TS model to fit the NiCo EIS data resulted in a very large disagreement between the experimental and CNLS approximations, but the use of the 2TP model gave a very good fit. According to the EEC parameter values presented in Table 3, the two time constants, τ_1 (CPE_1-R_1) and τ_2 (CPE_2-R_2), considerably decrease with overpotential and temperature, indicating that both semicircles are related to the kinetics of the process [51]. Both the Q_1 and the R_1 decrease with overpotential when the impedance data is fitted with the 2TP EEC model. Hence, the first time constant, τ_1 (C_1-R_1) or HF time constant, is related to the HER charge-transfer kinetics, namely to the response of double layer capacitance characterized by CPE_1, and HER charge transfer resistance characterized by R_1. On the other hand, the Q_2 and the R_2 rapidly decrease with overpotential, which is not consistent with a typical behavior associated with the response of the hydrogen adsorbed on an electrode surface [12, 29, 51, 53, 54]. Current results do not allow us to make a definite conclusion on the physical behaviour of the

LF time constant, but the overpotential trend of Q_2, α_2 and R_2, and their absolute values indicate that the observed LF response could be related to a response of some fast transfer processes (most likely charge, rather than mass) in a thin semiconducting oxide film layer formed on the NiCo surface [29]. As a result of the present analysis, it can be conclude that the 2TP EEC model is adequate to describe the impedance response of the NiCo alloy.

Besides the information on the kinetics of the HER, EIS results can be also used to estimate the real surface area of electrocatalytic coatings. This is important since by knowing the real electrochemically active area of the catalyst, it is possible to conclude on the intrinsic activity of the material in the HER, by subtracting for the surface area effect. Considering a value of 20 μF cm^{-2} for the double layer capacitance, C_{dl}, of a smooth nickel surface, used earlier in the literature [13, 37], the real active surface area, in terms of surface roughness factor (R_f), may be estimated by comparing the C_{dl} related to the HER charge-tranfer kinetics of porous/rough and smooth electrodes [6, 56]. The plots of the electrode surface roughness factor as function of the HER overpotential are displayed in Fig. 9. The R_f calculated values for the Ni-Hcd electrode are one order of magnitude higher than that reported for the NiCo catalyst. The R_f values of the latter, close to the unity, are in agreement with the smooth surface shown in Fig. 1.b, whereas the R_f values obtained for the Ni-Hcd catalyst reveals a larger surface, as a consequence of the pores and cavities. As it is clear from Fig. 9, the values of R_f decrease when increasing the cathodic potential. This indicates that a fraction of the inner surface of the electrode is blocked during HER due to gas bubbles shielding, and hence not electrochemically accessed by the electrolyte [6, 49, 60]. The R_f data allows us to evaluate the relative intrinsic catalytic activity of the investigated catalyst, by substracting the effect of the surface area. For this purpose, the Tafel plots were

normalized to the true surface area by dividing the curves by the corresponding surface roughness factor, see Fig. 10. Although previous data based on the geometric area (Fig.2 and Table 2) confirmed that Ni-Hcd yields the highest overall electrocatalytic activity in the HER, Fig. 10 and Table 4 show that the NiCo alloy presents a higher catalityc activity for the HER when the effect of the surface area is avoided. In Table 4 it is shown the exchange current densities, corrected with the surface roughness factor data, at different temperatures for the studied electrodes. The NiCo alloy improves in one order of magnitude the relative electrocatalytic activity for HER at $\eta \to 0$, compared to the smooth Ni electrode. In contrast, the Ni-Hcd has approximately the same exchange current density as the smooth Ni electrode, i. e. the same intrinsic catalytic activity at equilibrium conditions, which is obvious since in both cases the same electrocatalytic material was used (Ni). The other interesting observation derived from Fig. 10 is that, although both types of pure Ni electrodes show Tafelian dependencies of the same order of magnitude, their behaviours are different. At approximately $\eta >$ -200 mV the current density of the smooth electrode is slightly higher than that reported for the Ni-Hcd layer, while at $\eta <$ -200 mV the relationship is reversed due to the presence of an inflection point on the curve corresponding to the smooth nickel, which is not observed on the curve corresponding to the electrodeposited nickel. This effect can be explained by a different magnitude of the standard adsorption energy on the substrates analyzed. In the case of the smooth Ni electrode subjected to mechanical polishing the surface layer presents some degree of amorphization, which implies a disordered surface structure. On the contrary, the electrodes obtained by electrodeposition are highly crystalline and the surfaces have a more ordered structure. As a result, the polished nickel electrode shows a lower hydrogen equilibrium surface

coverage than the macroporous electrodeposits, which affects the hydrogen production at most cathodic overpotentials [22].

The increased intrinsic activity of the bicomponent NiCo catalyst in comparison to pure Ni is in accordance with literature [25]. It is well known that the HER electrocatalytic activity of Ni can be improved by the addition of a second metal into the alloy. A general conclusion found in the literature is that the intrinsic catalytic activity for the HER is related to the electronic structure of metals, although any explicit and comprehensive explanation has not yet been given. The theoretical approach in explaining the HER activity of alloy catalysis is even more complex, and several theories have been proposed. Lupi et al. postulated that in the case of Co concentrations ranging between 41 and 64 weight percent, the synergism among the catalytic properties of nickel (low hydrogen overpotential) and of cobalt (high hydrogen adsorption) is best realized and these phenomenon allows to obtain a larger value of exchange current density [25].

4. Conclusion

Electrocatalytic activity of pure Ni porous layers (Ni-Hcd electrode) and smooth NiCo alloys (47.7 wt. %) (NiCo electrode) produced by electrodeposition on AISI 304 stainless steel substrates was investigated in the hydrogen evolution reaction (HER).

Steady-state polarization curves and AC electrochemical impedance spectroscopy (EIS) measurements allowed us to determine the mechanism and kinetics of the HER. It was shown that the HER on both Ni-Hcd and NiCo catalysts is controlled by the Volmer reaction step as the rds (electrochemical adsorption of hydrogen to form $Ni\text{-}H_{ads}$).

EIS is a useful tool to determine the surface roughness factor, R_f, of the developed electrodes. Knowing this parameter it can be determined if the electrocatalytic activity of the studied materials is a result of only an increased surface area of the catalysts, or if an improvement in the intrinsic (electronic) electrocatalytic properties of the catalytic layer is a contributing factor.

Ni-Hcd catalyst yielded the highest overall electrocatalytic activity in the HER, mainly attributed to the increased surface area. Avoiding the surface roughness factor effect, Ni-Hcd catalyst manifested an intrinsic electrocatalytic activity similar to that reported for the smooth Ni electrode.

It was also clearly demonstrated that allowing Ni with Co results in an increased intrinsic electrocatalytic activity in the HER when compared to pure Ni. This phenomenon can be explained by a proper synergism among the catalytic properties of nickel (low hydrogen overpotential) and of cobalt (high hydrogen adsorption).

Acknowledgments

Isaac Herraiz-Cardona is grateful to the Ministerio de Ciencia e Innovación (Spain) for a postgraduate grant (Ref. AP2007-03737). This work was supported by Generalitat Valenciana (Project PROMETEO/2010/023)

References

[1] Veziroglu TN, Barbir F. Hydrogen - the wonder fuel. Int J Hydrogen Energy 1992;17:391-404.

[2] Elosta WB, Veziroglu TN. Solar hydrogen energy system for a Libyan coastal county. Int J Hydrogen Energy 1990;15:33-44.

[3] Bockris JO, Veziroglu TN. A solar-hydrogen economy for USA. Int J Hydrogen Energy 1983;8:323-340.

[4] Hug W, Divisek J, Mergel J, Seeger W, Steeb H. Highly efficient advanced alkaline electrolyzer for solar operation. Int J Hydrogen Energy 1992;17:699-705.

[5] Garciaconde AG, Rosa F. Solar hydrogen-production - A Spanish experience. Int J Hydrogen Energy 1993;18:995-1000.

[6] Kellenberger A, Vaszilcsin N, Brandl W, Duteanu N. Kinetics of hydrogen evolution reaction on skeleton nickel and nickel-titanium electrodes obtained by thermal arc spraying technique. Int J Hydrogen Energy 2007;32:3258-3265.

[7] Losiewicz B, Budniok A, Rowinski E, Lagiewka E, Lasia A. The structure, morphology and electrochemical impedance study of the hydrogen evolution reaction on the modified nickel electrodes. Int J Hydrogen Energy 2004;29:145-157.

[8] Krstajic NV, Jovic VD, Gajic-Krstajic L, Jovic BM, Antozzi AL, Martelli GN. Electrodeposition of Ni-Mo alloy coatings and their characterization as cathodes for hydrogen evolution in sodium hydroxide solution. Int J Hydrogen Energy 2008;33:3676-3687.

[9] Lasia A. Hydrogen Evolution. In: Vielstich W, Lamm A, Gasteiger HA, editors. Handbook of fuel cell technology, John Wiley and Sons Ltd; 2003, p. 416-440.

[10] Chen LL, Lasia A. Study of the kinetics of hydrogen evolution reaction on Nickel-Zinc powder electrodes. J Electrochem Soc 1992;139:3214-3219.

[11] Los P, Rami A, Lasia A. Hydrogen evolution reaction on Ni-Al electrodes. J Appl Electrochem 1993;23:135-140.

[12] Herraiz-Cardona I, Ortega E, Pérez-Herranz V. Impedance study of hydrogen evolution on Ni/Zn and Ni-Co/Zn stainless steel based electrodeposits. Electrochim Acta 2011;56:1308-1315.

[13] Chen LL, Lasia A. Study of the kinetics of hydrogen evolution reaction on Nickel-Zinc alloy electrodes. J Electrochem Soc 1991;138:3321-3328.

[14] Giz MJ, Machado SAS, Avaca LA, Gonzalez ER. High area Ni-Zn and Ni-Co-Zn codeposits as hydrogen electrodes in alkaline-solutions. J Appl Electrochem 1992;22:973-977.

[15] Giz MJ, Bento SC, Gonzalez ER. NiFeZn codeposit as a cathode material for the production of hydrogen by water electrolysis. Int J Hydrogen Energy 2000;25:621-626.

[16] Sheela G, Pushpavanam M, Pushpavanam S. Zinc-nickel alloy electrodeposits for water electrolysis. Int J Hydrogen Energy 2002;27:627-633.

[17] Suffredini HB, Cerne JL, Crnkovic FC, Machado SAS, Avaca LA. Recent developments in electrode materials for water electrolysis. Int J Hydrogen Energy 2000;25:415-423.

[18] Choquette Y, Brossard L, Lasia A, Menard H. Study of the kinetics of hydrogen evolution reaction on Raney-Nickel composite-coated electrode by AC impedance technique. J Electrochem Soc 1990;137:1723-1730.

[19] Choquette Y, Brossard L, Lasia A, Menard H. Investigation of hydrogen evolution on Raney-Nickel composite-coated electrodes. Electrochim Acta 1990;35:1251-1256.

[20] Okido M, Depo JK, Capuano GA. The mechanism of hydrogen evolution reaction on a modified Raney-Nickel composite-coated electrode by AC impedance. J Electrochem Soc 1993;140:127-133.

[21] Marozzi CA, Chialvo AC. Development of electrode morphologies of interest in electrocatalysis. Part 1: Electrodeposited porous nickel electrodes. Electrochim Acta 2000;45:2111-2120.

[22] Marozzi CA, Chialvo AC. Development of electrode morphologies of interest in electrocatalysis: Part 2: Hydrogen evolution reaction on macroporous nickel electrodes. Electrochim Acta 2001;46:861-866.

[23] Vazquez-Gomez L, Cattarin S, Guerriero P, Musiani M. Preparation and electrochemical characterization of Ni + RuO_2 composite cathodes of large effective area. Electrochim Acta 2007;52:8055-8063.

[24] Huang YJ, Lai CH, Wu PW, Chen LY. Ni inverse opals for water electrolysis in an alkaline electrolyte. J Electrochem Soc 2010;157:18-22.

[25] Lupi C, Dell'Era A, Pasquali M. Nickel-cobalt electrodeposited alloys for hydrogen evolution in alkaline media. Int J Hydrogen Energy 2009;34:2101-2106.

[26] Solmaz R, Döner A, Sahin I, Y³ce AO, Kardas G, Yazici B, Erbil M. The stability of NiCoZn electrocatalyst for hydrogen evolution activity in alkaline solution during long-term electrolysis. Int J Hydrogen Energy 2009;34:7910-7918.

[27] Han Q, Chen J, Liu K, Li X, Wei X. The heat-treatment effect of amorphous Ni-S(La) term electrode on the hydrogen evolution reaction in an alkaline media. Int J Hydrogen Energy 2004;29:597-603.

[28] Domínguez-Crespo MA, Torres-Huerta AM, Brachetti-Sibajab B, Flores-Vela A. Electrochemical performance of Ni-RE (RE = rare earth) as electrode material for hydrogen evolution reaction in alkaline medium. Int J Hydrogen Energy 2011;36:135-151.

[29] Navarro-Flores E, Chong ZW, Omanovic S. Characterization of Ni, NiMo, NiW and NiFe electroactive coatings as electrocatalysts for hydrogen evolution in an acidic medium. J Mol Cat A: Chemical 2005;226:179-197.

[30] Aaboubi O. Hydrogen evolution activity of Ni-Mo coating electrodeposited under magnetic field control. Int J Hydrogen Energy 2011;36:4702-4709.

[31] Rashkov R, Arnaudova M, Avdeev G, Zielonka A, Jannakoudakis P, Jannakoudakis A, Theodoridou E. NiW/TiO_x composite layers as cathode material for hydrogen evolution reaction. Int J Hydrogen Energy 2009;34:2095-2100.

[32] Solmaz R, Kardas G. Electrochemical deposition and characterization of NiFe coatings as electrocatalytic materials for alkaline water electrolysis. Electrochim Acta 2009;54:3726-3734.

[33] García-Antón J, Blasco-Tamarit E, García-García DM, Guiñón-Pina V, Leiva-García R, Pérez-Herranz V. 2008: P200803389.

[34] Southampton Electrochemistry Group. Instrumental Methods in Electrochemistry. New York: Wiley; 1985.

[35] Chen LL, Lasia A. Hydrogen evolution reaction on Nickel-Molybdenum powder Electrodes. J Electrochem Soc 1992;139:3458-3464.

[36] J. O. Bockris and A. K. N. Reddy. Modern Electrochemistry.2nd ed. New York: Kluwer/Plenum Press; 2000.

[37] Rami A, Lasia A. Kinetics of hydrogen evolution on Ni-Al Alloy electrodes. J Appl Electrochem 1992;22:376-382.

[38] Angelo ACD, Lasia A. Surface effects in the hydrogen evolution reaction on Ni-Zn Alloy electrodes in alkaline-solutions. J Electrochem Soc 1995;142:3313-3319.

[39] Highfield JG, Claude E, Oguro K. Electrocatalytic synergism in Ni/Mo cathodes for hydrogen evolution in acid medium: a new model. Electrochim Acta 1999;44:2805-2814.

[40] Kaninski MPM, Nikolic VM, Potkonjak TN, SimonoviccBR, Potkonjak NI. Catalytic activity of Pt-based intermetallics for the hydrogen production - Influence of ionic activator. Appl Cat A: General 2007;321:93-99.

[41] Metikos-Hukovic A, Grubac Z, Radic N, Tonejc A. Sputter deposited nanocrystalline Ni and Ni-W films as catalysts for hydrogen evolution. J Mol Cat A: Chemical 2006;249:172-180.

[42] Rosalbino F, Delsante S, Borzone G, Angelini E. Electrocatalytic behaviour of Co-Ni-R (R=Rare earth metal) crystalline alloys as electrode materials for hydrogen evolution reaction in alkaline medium. Int J Hydrogen Energy 2008;33:6696-6703.

[43] Lasia A, Rami A. Kinetics of hydrogen evolution on Nickel electrodes. J Electroanal Chem 1990;294:123-141.

[44] Dominquez-Crespo MA, Ramirez-Meneses E, Montiel-Palma V, Huerta AMT, Rosales HD. Synthesis and electrochemical characterization of stabilized nickel nanoparticles. Int J Hydrogen Energy 2009;34:1664-1676.

[45] Krstajic N, Trasatti S. Cathodic behaviour of RuO_2-doped Ni/Co_3O_4 electrodes in alkaline solutions: hydrogen evolution. J Appl Electrochem 1998;28:1291-1297.

[46] Shervedani RK, Madram AR. Electrocatalytic activities of nanocomposite $Ni_{81}P_{16}C_3$ electrode for hydrogen evolution reaction in alkaline solution by electrochemical impedance spectroscopy. Int J Hydrogen Energy 2008;33:2468-2476.

[47] Harrington DA, Conway BE. AC Impedance of Faradaic reactions involving electrosorbed intermediates--I. Kinetic theory. Electrochim Acta 1987;32:1703-1712.

[48] Paseka I. Hydrogen evolution reaction on amorphous Ni-P and Ni-S electrodes and the internal stress in a layer of these electrodes. Electrochim Acta 2001;47:921-931.

[49] Ganesh V, Lakshminarayanan V. Preparation of high surface area nickel electrodeposit using a liquid crystal template technique. Electrochim Acta 2004;49:3561-3572.

[50] Armstrong RD, Henderson M. Impedance plane display of a reaction with an adsorbed intermediate. J Electroanal Chem 1972;39:81-90.

[51] Birry L, Lasia A. Studies of the hydrogen evolution reaction on Raney nickel-molybdenum electrodes. J Appl Electrochem 2004;34:735-749.

[52] Growcock FB, Jasinski RJ. Time-Resolved Impedance Spectroscopy of Mild-Steel in Concentrated Hydrochloric-Acid. J Electrochem Soc 1989;136:2310-2314.

[53] Simpraga R, Tremiliosi-Filho G, Qian SY, Conway BE. In situ determination of the 'real are factor' in H_2 evolution electrocatalysis at porous Ni---Fe composite electrodes. J Electroanal Chem 1997;424:141-151.

[54] Castro EB, Giz MJ, Gonzalez ER, Vilche JR. An electrochemical impedance study on the kinetics and mechanism of the hydrogen evolution reaction on nickel molybdenite electrodes. Electrochim Acta 1997;42:951-959.

[55] Borresen B, Hagen G, Tunold R. Hydrogen evolution on $Ru_xTi_{1-x}O_2$ in 0.5 M H_2SO_4. Electrochim Acta 2002;47:1819-1827.

[56] Kubisztal J, Budniok A, Lasia A. Study of the hydrogen evolution reaction on nickel-based composite coatings containing molybdenum power. Int J Hydrogen Energy 2007;32:1211-1218.

[57] Brug GJ, Vandeneeden ALG, Sluytersrehbach M, Sluyters JH. The analysis of electrode impedances complicated by the presence of a constant phase element. J Electroanal Chem 1984;176:275-295.

[58] Hitz C, Lasia A. Experimental study and modeling of impedance of the her on porous Ni electrodes. J Electroanal Chem 2001;500:213-222.

[59] Orazem ME, Pebere N, Tribollet B. Enhanced graphical representation of electrochemical impedance data. J Electrochem Soc 2006;153:B129-B136.

[60] Pierozynski B, Smoczynski L. Kinetics of hydrogen evolution reaction at Nickel-Coated carbon fiber materials in 0.5 M H_2SO_4 and 0.1 M NaOH solutions. J Electrochem Soc 2009;156:B1045-B1050.

LIST OF TABLES

LIST OF FIGURES

Table 1. Experimental conditions used in the electrodeposition of electrocatalytic coatings on an AISI 304 stainless steel substrate.

Catalyst			
Ni-Hcd			
	Current density (mA cm^{-2})		1000
	Duration (hour)		1
	Bath composition (g L^{-1})	$NiCl_2 \cdot 6(H_2O)$	48
		NH_4Cl_2	170
	Temperature (ºC)		25
NiCo			
	Current density (mA cm^{-2})		30
	Duration (hour)		5
	Bath composition (g L^{-1})	$NiSO_4 \cdot 6(H_2O)$	170
		$CoSO_4 \cdot 6(H_2O)$	22
		H_3BO_3	20
	Temperature (ºC)		60

Table 2. Kinetic parameters of the HER obtained from the polarization curves recorded in 30 % wt KOH solution at different temperatures.

Catalyst		Temperature (ºC)					
		30	40	50	60	70	80
Smooth Ni							
	***b* (mV dec^{-1})**	97.9	103.7	107.5	122.8	137.3	171.4
	i_0 (μA cm^{-2})	0.07	0.16	0.44	0.92	2.00	4.77
	β	0.61	0.60	0.60	0.54	0.50	0.41
	η_{100} (mV)	503	496	470	496	502	555
Ni-Hcd							
	***b* (mV dec^{-1})**	100.0	108.2	111.0	121.6	120.8	133.5
	i_0 (μA cm^{-2})	8.2	15.8	16.4	37.0	43.1	70.1
	β	0.60	0.57	0.58	0.54	0.56	0.52
	η_{100} (mV)	309	300	306	293	284	285
NiCo							
	***b* (mV dec^{-1})**	100.8	111.4	122.3	135.6	139.5	145.0
	i_0 (μA cm^{-2})	5.7	5.0	5.8	9.3	16.5	21.4
	β	0.60	0.56	0.52	0.49	0.49	0.48
	η_{100} (mV)	334	386	402	414	390	339

Table 3. EEC parameters obtained by fitting EIS experimental spectra recorded at various overpotentials on the investigated electrocatalytic coatings using the EEC models presented in Fig.5.

Catalyst	Temperature (°C)								
	30			50			80		
Ni-Hcd									
	2TS EEC								
	η_1	η_2	η_3	η_1	η_2	η_3	η_1	η_2	η_3
χ^2	$9.45\cdot10^{-4}$	$7.69\cdot10^{-4}$	$3.24\cdot10^{-4}$	$6.00\cdot10^{-4}$	$4.85\cdot10^{-4}$	$4.47\cdot10^{-4}$	$5.86\cdot10^{-4}$	$2.19\cdot10^{-4}$	$1.26\cdot10^{-4}$
R_S (Ω cm^2)	0.66	0.66	0.66	0.48	0.46	0.49	0.36	0.37	0.36
R_1 (Ω cm^2)	4.61	5.55	6.41	3.41	3.80	3.76	1.14	1.25	1.38
R_2 (Ω cm^2)	362.0	187.5	11.7	184.0	80.0	8.0	53.6	26.5	4.2
Q_1 (mΩ^{-1} cm^{-2} s^n)	9.51	6.07	3.89	8.65	6.68	3.59	10.26	9.69	8.16
n_1	0.82	0.83	0.83	0.83	0.82	0.86	0.76	0.76	0.75
C_1 (mF cm^{-2})*	2.99	1.91	1.13	2.69	1.80	1.20	2.01	1.44	1.06
Q_2 (mΩ^{-1} cm^{-2} s^n)	14.4	10.8	7.9	12.9	8.8	8.2	10.9	8.1	6.9
n_2	0.92	0.95	0.99	0.92	0.95	0.94	0.92	0.94	0.94
C_2 (mF cm^{-2})*	11.5	9.3	7.6	9.9	7.4	6.4	7.5	6.1	5.1
τ_1 (s) #	$4.4\cdot10^{-2}$	$3.4\cdot10^{-2}$	$2.5\cdot10^{-2}$	$3.0\cdot10^{-2}$	$2.6\cdot10^{-2}$	$1.4\cdot10^{-2}$	$1.4\cdot10^{-2}$	$1.2\cdot10^{-2}$	$1.1\cdot10^{-2}$
τ_2 (s) #	$4.1\cdot10^{0}$	$1.7\cdot10^{0}$	$8.9\cdot10^{-2}$	$1.8\cdot10^{0}$	$6.0\cdot10^{-1}$	$5.1\cdot10^{-2}$	$4.0\cdot10^{-1}$	$1.6\cdot10^{-1}$	$2.1\cdot10^{-2}$
NiCo									
	2TP EEC								
	η_1	η_2	η_3	η_1	η_2	η_3	η_1	η_2	η_3
χ^2	$7.01\cdot10^{-4}$	$3.49\cdot10^{-4}$	$9.15\cdot10^{-5}$	$1.93\cdot10^{-4}$	$1.07\cdot10^{-4}$	$7.61\cdot10^{-4}$	$2.45\cdot10^{-3}$	$9.06\cdot10^{-4}$	$1.19\cdot10^{-3}$
R_S (Ω cm^2)	0.81	0.79	0.81	0.54	0.54	0.56	0.38	0.37	0.39
R_1 (Ω cm^2)	68.2	64.7	27.7	49.3	36.2	22.5	23.8	18.8	12.3
R_2 (Ω cm^2)	$4.3\cdot10^{3}$	$2.5\cdot10^{3}$	$9.3\cdot10^{1}$	$2.8\cdot10^{3}$	$5.6\cdot10^{2}$	$7.9\cdot10^{1}$	$7.8\cdot10^{2}$	$1.7\cdot10^{2}$	$4.0\cdot10^{1}$
Q_1 (mΩ^{-1} cm^{-2} s^n)	0.98	0.88	0.39	0.80	0.46	0.24	0.56	0.30	0.19
n_1	0.89	0.89	0.92	0.89	0.91	0.94	0.90	0.91	0.93
C_1 (mF cm^{-2})*	0.41	0.37	0.19	0.29	0.19	0.13	0.21	0.12	0.09
Q_2 (mΩ^{-1} cm^{-2} s^n)	2.14	2.07	1.05	3.48	2.62	1.00	6.30	3.56	1.56
n_2	0.41	0.42	0.34	0.39	0.41	0.58	0.40	0.44	0.57
C_2 (mF cm^{-2})*	$1.38\cdot10^{-1}$	$1.32\cdot10^{-1}$	$7.63\cdot10^{-4}$	$2.26\cdot10^{-1}$	$8.04\cdot10^{-2}$	$5.65\cdot10^{-2}$	$3.48\cdot10^{-1}$	$9.47\cdot10^{-2}$	$6.87\cdot10^{-2}$
τ_1 (s) #	$2.8\cdot10^{-2}$	$2.4\cdot10^{-2}$	$5.2\cdot10^{-3}$	$1.4\cdot10^{-2}$	$6.9\cdot10^{-3}$	$3.0\cdot10^{-3}$	$5.1\cdot10^{-3}$	$2.0\cdot10^{-3}$	$1.1\cdot10^{-3}$
τ_2 (s) #	$6.0\cdot10^{-1}$	$3.3\cdot10^{-1}$	$7.1\cdot10^{-5}$	$6.3\cdot10^{-1}$	$4.5\cdot10^{-2}$	$4.5\cdot10^{-3}$	$2.7\cdot10^{-1}$	$1.6\cdot10^{-2}$	$2.8\cdot10^{-3}$

* Calculated using Eq. 8

Calculated from the best-fit estimates of EEC parameters.

Table 4. Exchange current densities ($\mu A\ cm^{-2}$) corrected with the surface roughness factor obtained from the polarization curves recorded in 30 % wt. KOH solution at different temperatures.

	Catalyst		
Temperature (°C)	**Smooth Ni**	**Ni-Hcd**	**NiCo**
30	0.07	0.14	2.80
40	0.16	0.30	2.87
50	0.44	0.33	3.96
60	0.92	0.82	6.90
70	2.00	1.04	13.92
80	4.77	1.88	20.11

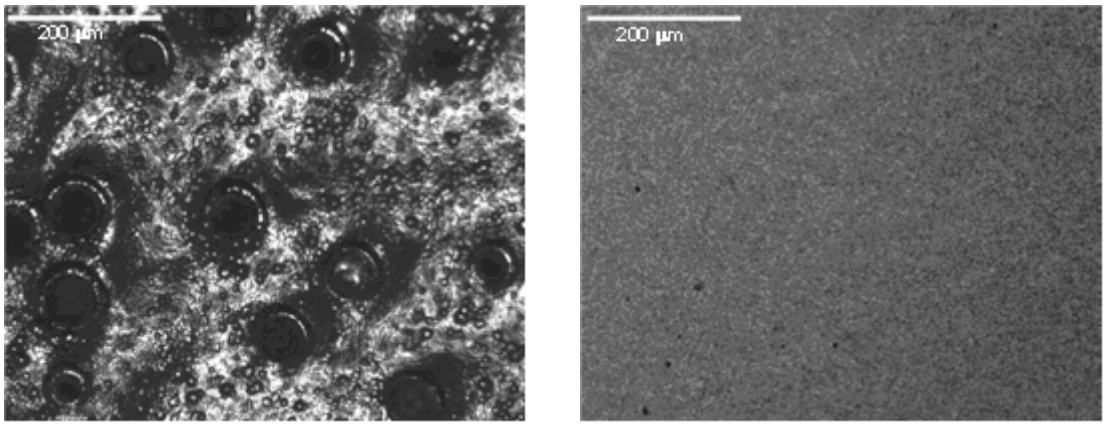

(a) **(b)**

Figure 1. Scanning electron micrographs of the (a) Ni-Hcd and (b) NiCo catalysts.

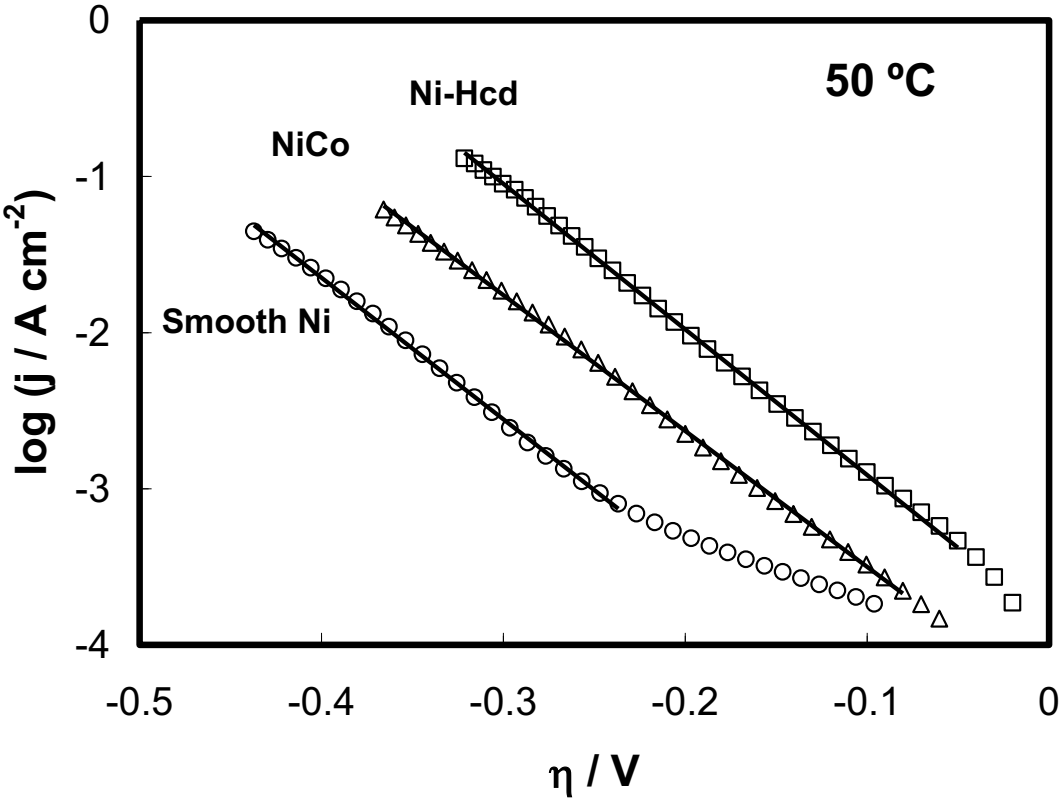

Figure 2. Linear Tafel polarization curves recorded on Ni-Hcd, NiCo, and smooth Ni electrocatalysts in 30 % wt KOH solution at 50 ºC.

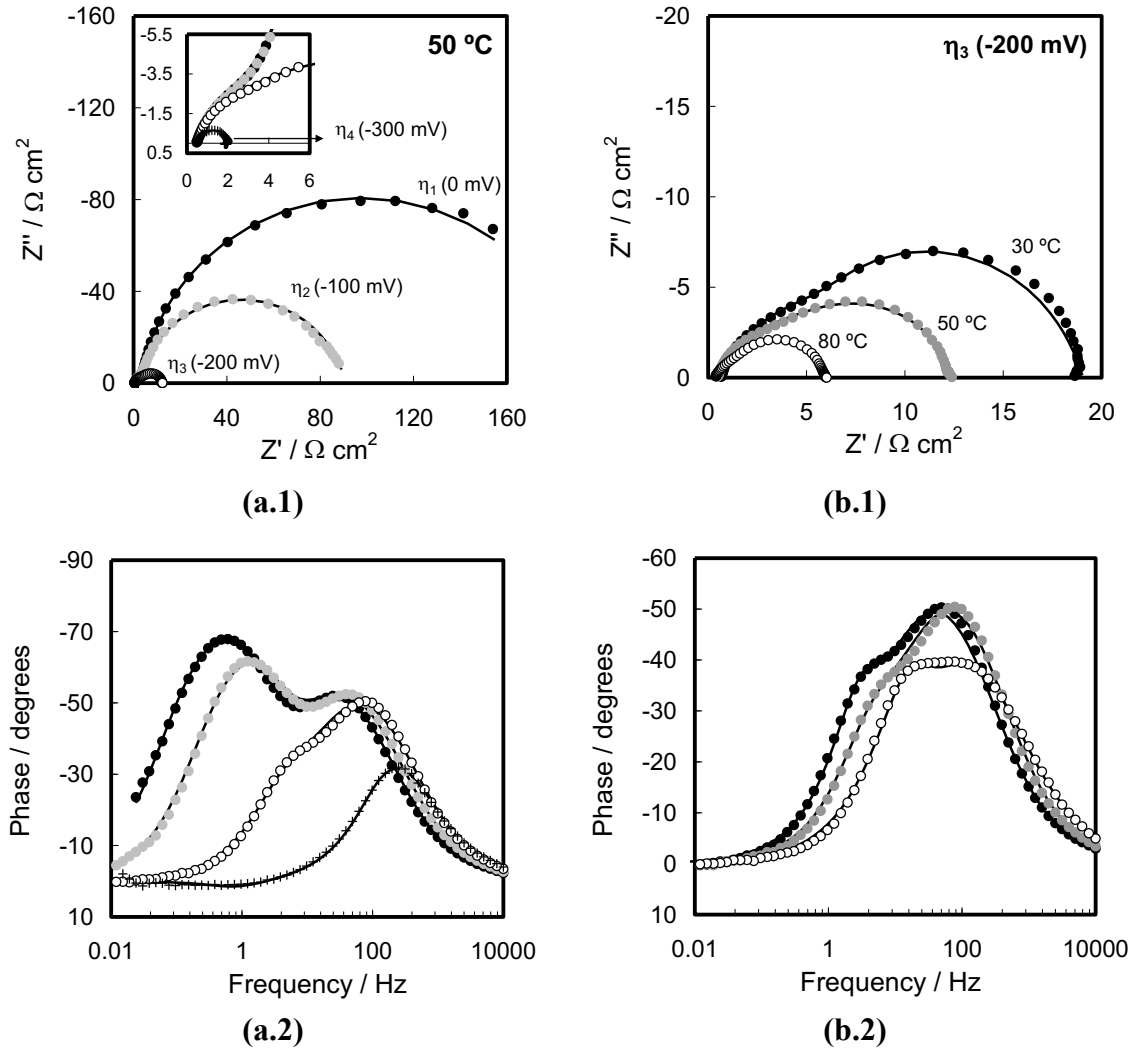

Figure 3. Impedance data obtained for the Ni-Hcd catalyst in 30 % wt. KOH solution at: (a) 50 ºC (Effect of overpotential): (a.1) Nyquist representation, (a.2) Bode representation of the phase angle as a function of frequency; and at overpotential η_3 (Effect of temperature): (b.1) Nyquist representation, (b.2) Bode representation of the phase angle as a function of frequency. The lines represent the measurement model fit to the impedance data sets.

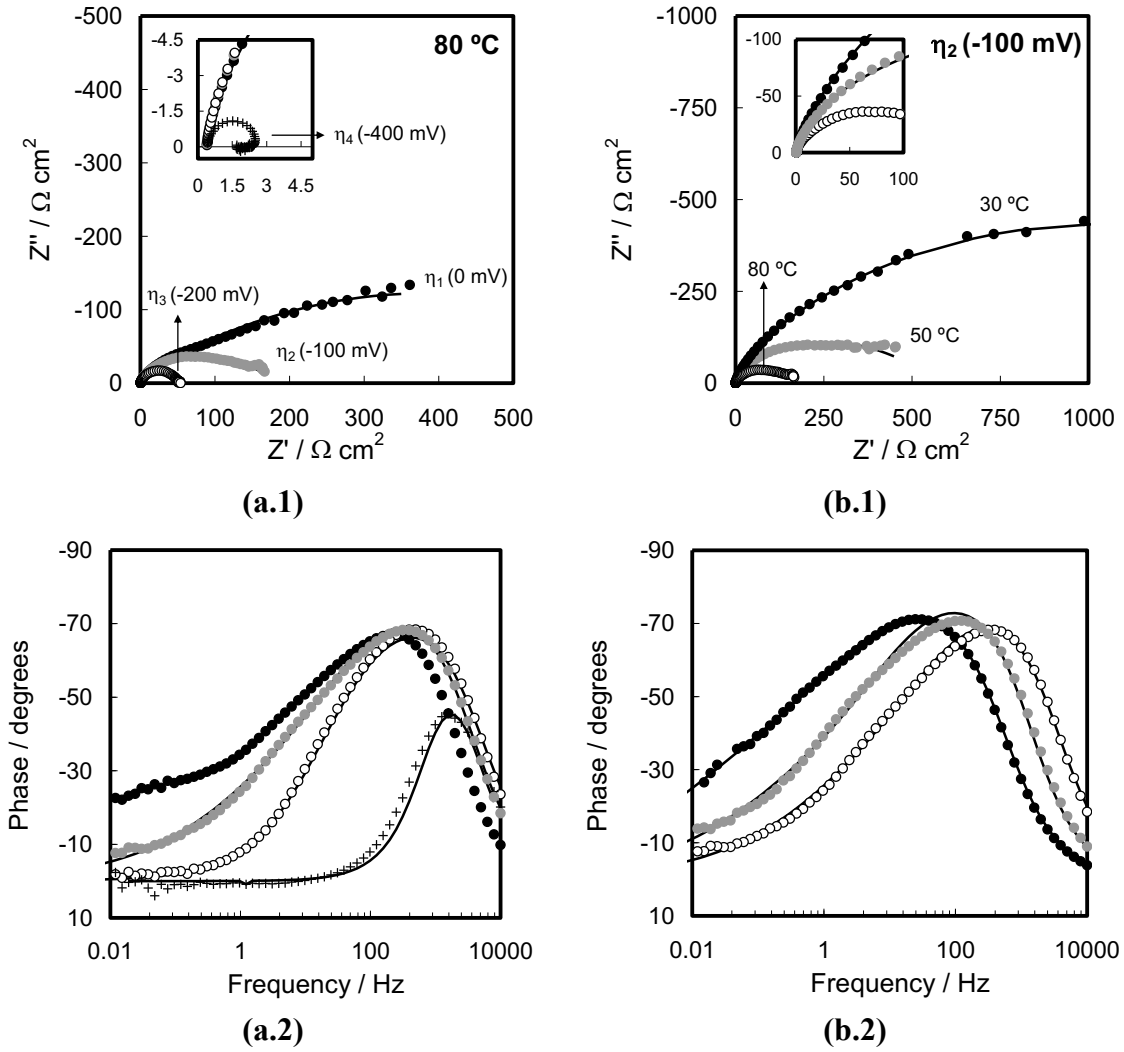

Figure 4. Impedance data obtained for the NiCo catalyst in 30 % wt. KOH solution at: (a) 80 ºC (Effect of overpotential): (a.1) Nyquist representation, (a.2) Bode representation of the phase angle as a function of frequency; and at overpotential η_2 (Effect of temperature): (b.1) Nyquist representation, (b.2) Bode representation of the phase angle as a function of frequency. The lines represent the measurement model fit to the impedance data sets.

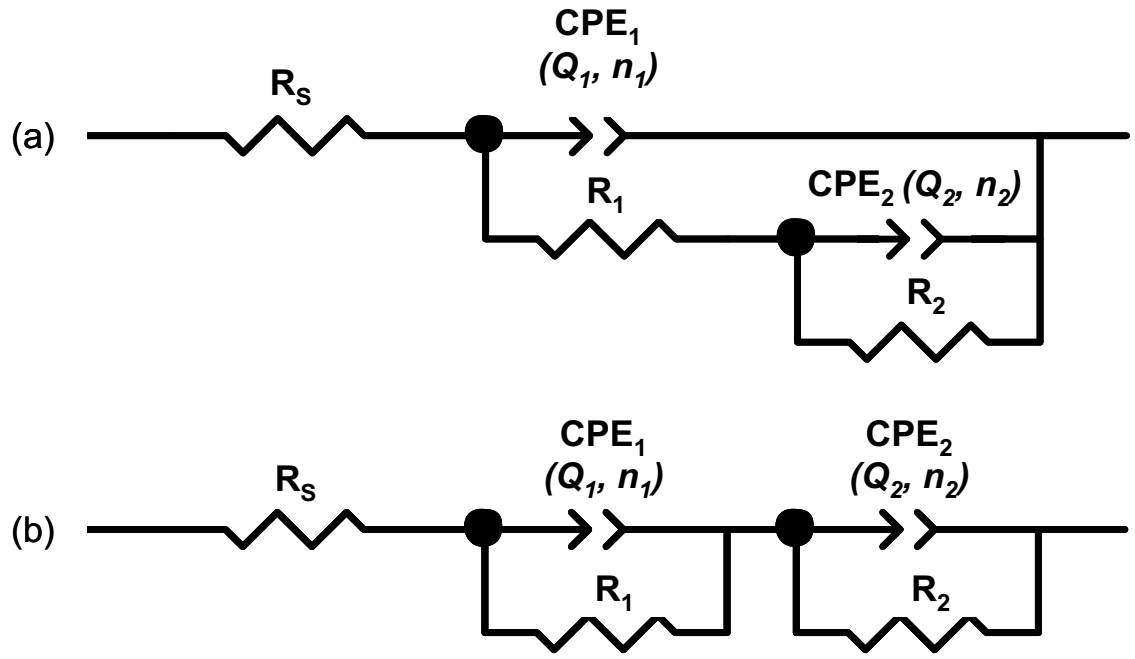

Figure 5. EEC models used to explain the EIS response of the HER on the Ni-Hcd and NiCo: (a) two-time constant parallel model (2TP), and (b) two time constant serial model (2TS).

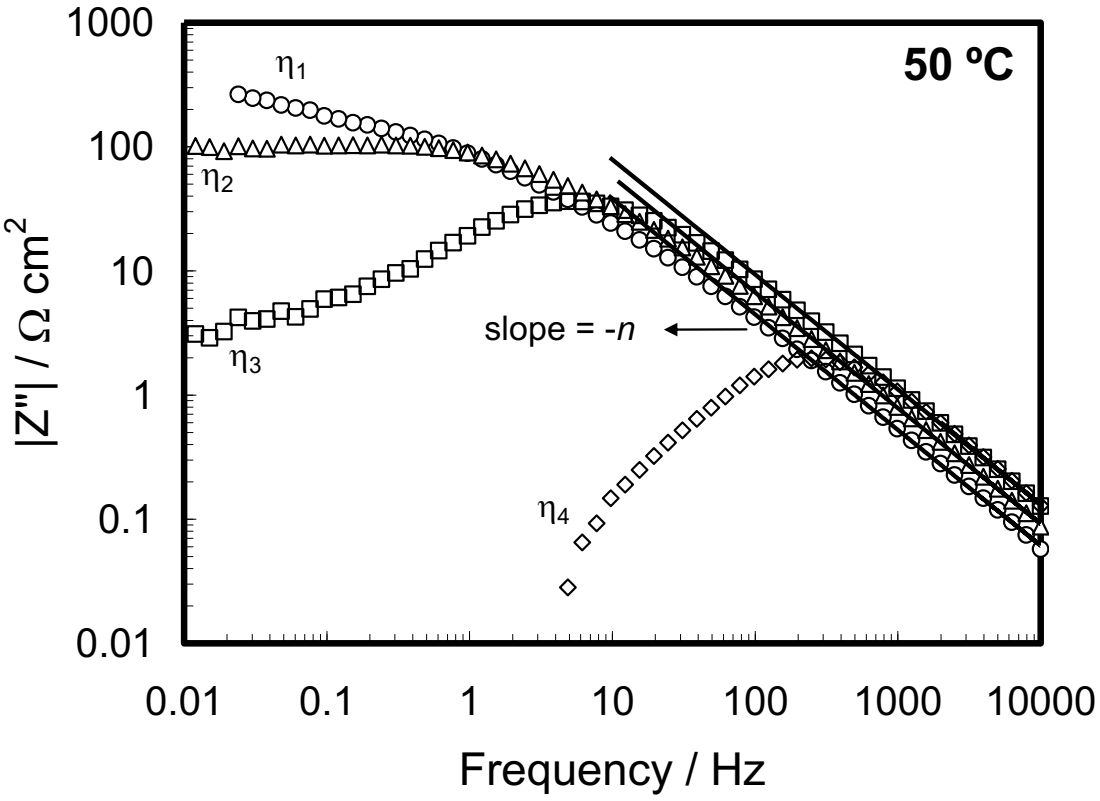

Figure 6. Imaginary part of the impedance as a function of frequency for the NiCo catalyst at 50 ºC and at different overpotential values in 30 % wt. KOH solution. The lines were fitted to the high –frequency data for the different overpotentials.

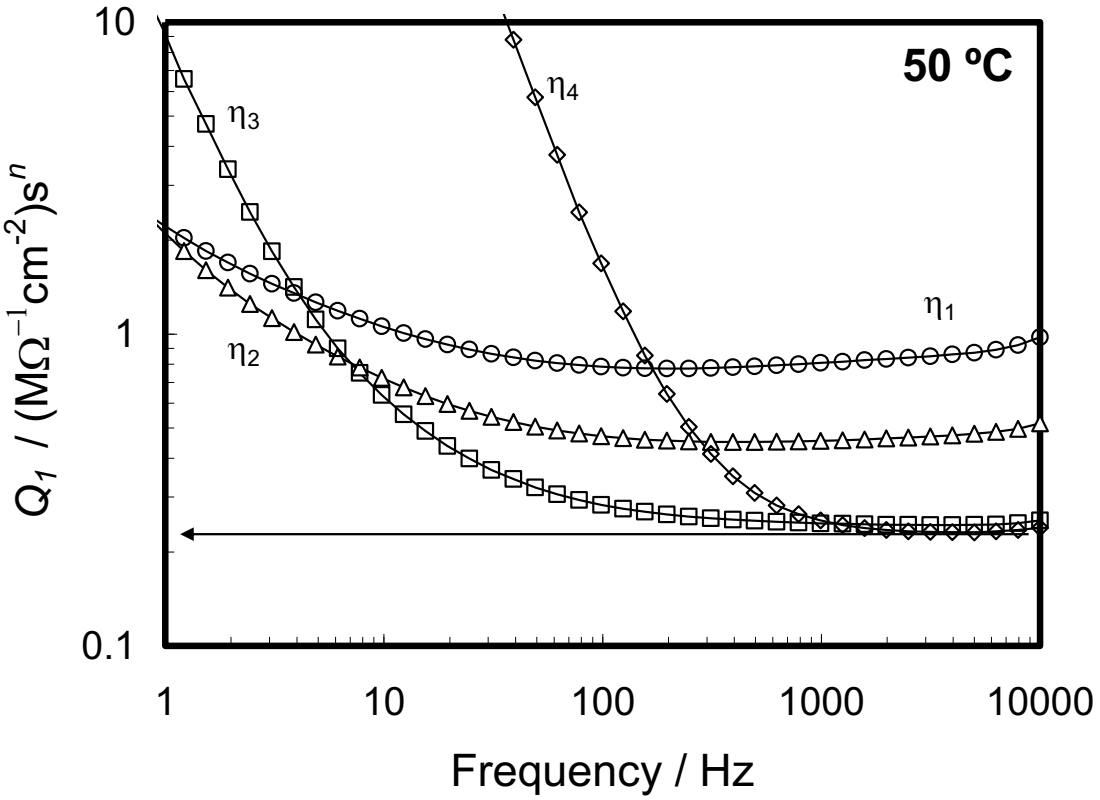

Figure 7. Effective CPE coefficient, Q_1, defined by Eq. 9 for the NiCo catalyst at 50 ºC and at different overpotential values in 30 % wt. KOH solution.

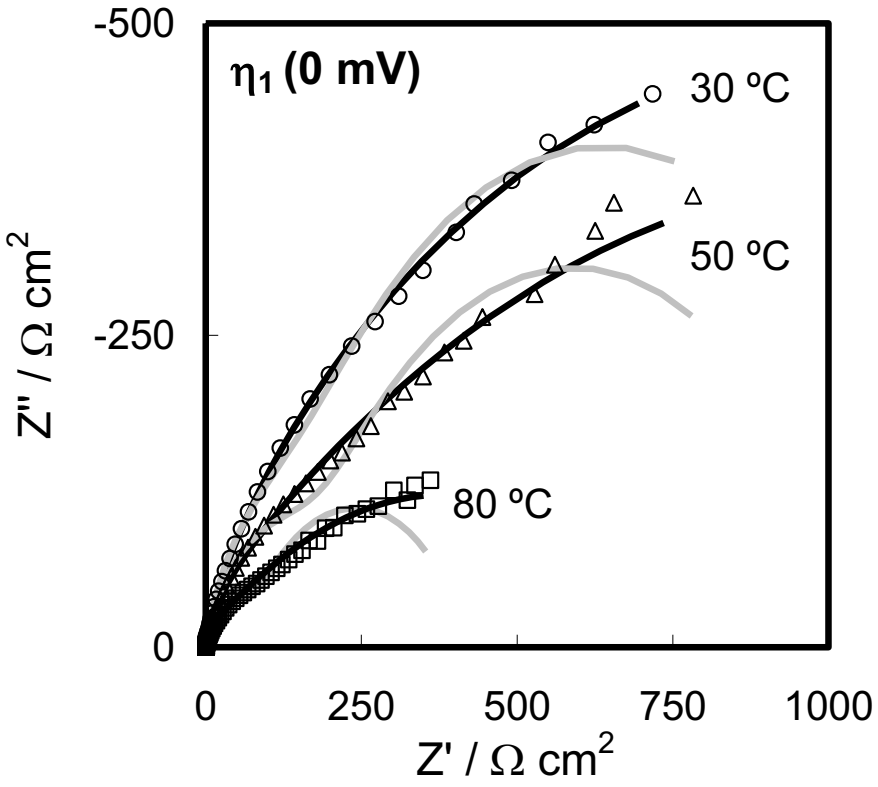

Figure 8. Nyquist plots obtained for the NiCo catalyst at η_1 and different temperatures in 30 % wt. KOH solution. Comparison between the 2TP EEC (black lines) and 2TS EEC (grey lines).

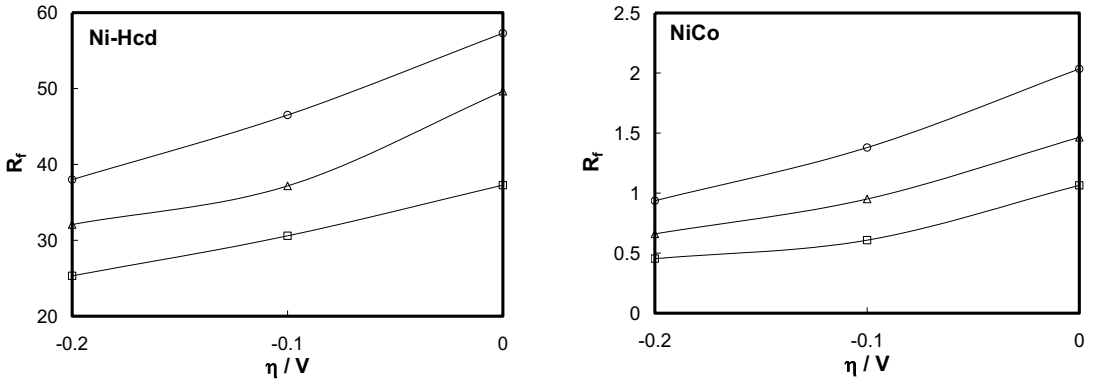

Figure 9. Surface roughness factor, R_f, as a function of the overpotential for the developed electrodes in 30 % wt. KOH solution at: ○ 30 ºC, △ 50 ºC, and □ 80 ºC.

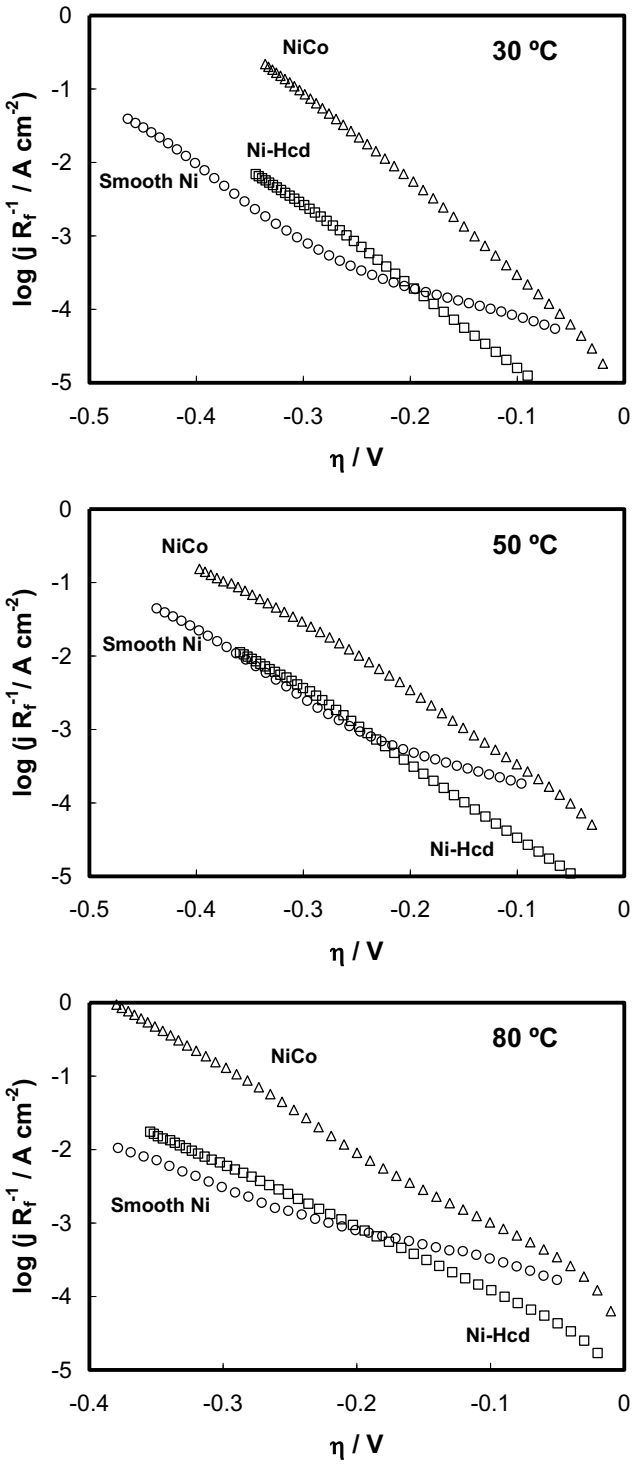

Figure 10. Linear Tafel polarization curves recorded on Ni-Hcd, NiCo, and smooth Ni electrocatalysts in 30 % wt. KOH solution at different temperatures, corrected considering the surface roughness factor, R_f,.